INVESTIGATION OF THE WALL PRESSURE FLUCTUATIONS, THE OPERATIONAL DEFLECTION SHAPES AND THE AIRBORNE NOISE RADIATION OF A SINGLE STAGE RADIAL PUMP

M. Witte, O. Kranz, B. Torner and F.-H. Wurm

Institute of Turbomachinery, Albert-Einstein-Straße 2, 18059 Rostock, Germany

ABSTRACT

The emission of hydro acoustic and airborne noise is a crucial aspect for pump applications in building equipment systems. Hydrodynamic pressure fluctuations inside the pump are the source for the noise emission. These fluctuations propagate far into the connected pipe system as hydro acoustic pressure waves. Furthermore, they will excite structural vibrations of the pump housing causing the emission of airborne noise in the vicinity. The experimental determination of the wall pressure fluctuations, the operational deflection shapes (ODS) as well the airborne noise emissions are one part of this study. The main part of this study will focus on the development and test of a new software framework combining a scale resolving flow simulation and finite element simulation for the numerically prediction of the ODS. The comparison of the computed ODS with the experiment at the 1th and 2th order of the blade passing frequency confirmed a good accordance.

KEYWORDS

UNSTEADY FLOWS, FLOW INDUCED VIBRATION, FLOW INDUCED NOISE

NOMENCLATURE

d_1	hub diameter [m]	t	time [s]
d_2	rotor diameter [m]	U_2	circumferential rotor speed at d_2 [m/s]
Q	flow rate [m^3/h]	Q*	Hunt's vortex criterion [s^{-2}]
y^+	dimensionless wall distance [-]	RMS	root mean square
Δt	time step width [s]		
u_i	i =x,y,z displacement [m]		
ρ	density [kg/m^3]		
H	head [m]		
p	pressure [Pa]		
f	frequency [Hz]		
n	rotational speed [min^{-1}]		
y^+	dimensionless wall distance [-]		

INTRODUCTION

Pumps are basic elements in complex hydraulic networks of building equipment systems, in oil and gas plants, chemical plants or either in transportation systems where they are mostly used for cooling purposes. The hydraulic efficiency is surely an important factor for all pumps but especially in the range of building equipment systems other claims have to be considered as well. The

requirements for those application fields in terms of hydroacoustic and airborne noise emissions are enhanced not only by stricter official regulations but also by customer expectations. It is obvious that the reduction of noise emission is turning more and more into the focus. Investigations have been already done in the past to enhance the understanding of the noise generation and emission process for different types of turbomachinery and for different application purposes. Strub (1964) for example investigated experimentally the pressure fluctuations in storage pumps and pump turbines. The full scale or model pumps were equipped with piezo-quartz pickups to record the pressure pulsation in the volute. The experiments were flanked by analytical models which were capable to predict the most pronounced frequency components in the pressure field from the interaction between rotor blades and guide vanes blades. Strub conclude that a proper choice of the number of rotor and guide vanes blades will have on important influence on the pressure pulsations of the pump. In the context of the space race in the middle of the 20th century a lot of fundamental investigations were initiated to understand pressure oscillations in the fuel and propulsion system in rocket engines. Jackson (1966) investigated the discharge pressure oscillations of the Mark 10 and Mark 26 fuel pumps. The Mark 10 was used in the first stage of the famous Saturn 5 rocket to fed the thrust chamber with RP-1 propellant and liquid oxygen. The Mark 26 was planned as a replacement for the existing cryogenic axial fuel pumps of the second stage. The development of new numerical procedures for the prediction of wake, cavitation and stall induced pressure oscillations and the comparison with experimental validation data was the main objective of Jackson's study. The usage of Computational Fluid Dynamic (CFD) methods has become more and more important as computer technology advances.

Berten et al. (2007) investigated the unsteady pressure pulsations by the rotor – stator interaction in a multi stage radial pump with a k-ω-SST URANS simulation. The unsteady pressure pulsations from the URANS were fed into a 1D pipeline model to solve the inhomogeneous wave equation. It could be shown in combination of both methods that acoustic modes were excited in the volute casing of the pump. Langthjem and Olhoff (2004) investigated the hydro acoustic noise emission inside of a radial pump by using a BEM method to model the transient pressure field as source term for the solution of the inhomogeneous wave equations. The interaction between the tongue and the rotor of a radial pump were in the scope of the experimental investigations by Dong et al. (1997). The authors combined the Particle Image Velocimetry (PIV) and wall pressure measurements to analyze the jet flow characteristics from the rotor outlet in the vicinity of the tongue. The main conclusion of this work was that an increase of the gap between tongue and rotor reduces the amplitudes of the pressure pulsations thus it is beneficial for the reduction of the noise emission.

Darvish et al. (2015) investigated design variations of the tongue of a radial blower with respect to the influence on the noise emission. They used a Large Eddy Simulation (LES) to compute the unsteady pressure and velocity fields as input data for the acoustic field calculation with an acoustic analogy method.

The influence of coherent flow structures in the rotor - stator gap of an axial fan were investigated by Zhu et al. (2016) by using a compressible Lattice Boltzmann Method (LBM) in combination with comprehensive experiments to obtain sound pressure data as well as wall pressure data from the blades. The authors were capable to show that several humps in the acoustic spectrum are related to coherent flow structures in the gap. They identified pressure modes in the gap which were rotating at around 30% of the rotor speed in the same direction. The most relevant modes were multiples of the blade number.

The Proper Orthogonal Decomposition (POD) of the unsteady pressure and velocity fields in the volute of a radial pump was done by Witte et al. (2018). The POD input data were computed with a scale resolving k-ω SST SAS simulation. Several coherent flow structures assigned to different orders of the blade passing frequency (BPF) making them relevant for the noise emission have been identified and topologically explained. The BPF is defined is the rotational frequency of the rotor multiply by the blade number.

So far, we can conclude that a lot of investigations have been done in the past and a lot more are in progress. In the case of a radial pump we are faced with the challenges that two different types of noise emission have to put in consideration. Pressure pulsations by the rotor – stator interaction are the source for both of these two emission types. These pulsations in the pressure field will propagate far into the connected pipe system as hydroacoustic pressure waves. Depending on the mechanical properties of the pipe system and the connected secondary devices natural frequencies of the pipe system can be excited causing the emission of noise far away from the pump itself. Additionally, wall pressure fluctuations inside the pump excite vibrations of the housing and will therefore fire up the airborne noise emission in the vicinity of the pump.
A comprehensive chain of different numerical procedures is needed but currently not available for the simulation of the airborne noise emission of a pump. The development of the combined procedures is the topic of a project with industrial and university partners. In the present study we will show the current state onto the way of the numerical prediction of the airborne noise emission of a pump. A comprehensive experimental setup has been developed for this purpose by Witte et al. (2016) and Bleeck et al. (2016) to investigate the hydroacoustic and airborne noise emission of a single stage radial pump. The study will focus on the experimental and numerical investigations of the operational deflection shapes (ODS) of the pump under operating conditions. The operational deflection shapes respectively the surface normal component of the vibration velocity of the pump casing is most important for the airborne noise emission. Especially, the ODS determines the acoustic radiation pattern from the pump depending on the frequency. The input data for the numerical guided ODS analysis of the pump by Finite Element Method (FEM) were extracted in terms of wall pressure fields from a scale resolving k-ω SST SAS simulation. The investigations were flanked by experimental dynamic wall pressure measurement in the volute and side chambers of the pump as well as the measurement of the airborne noise emission of the pump inside the semi - anechoic test chamber.

EXPERIMENTAL SETUP

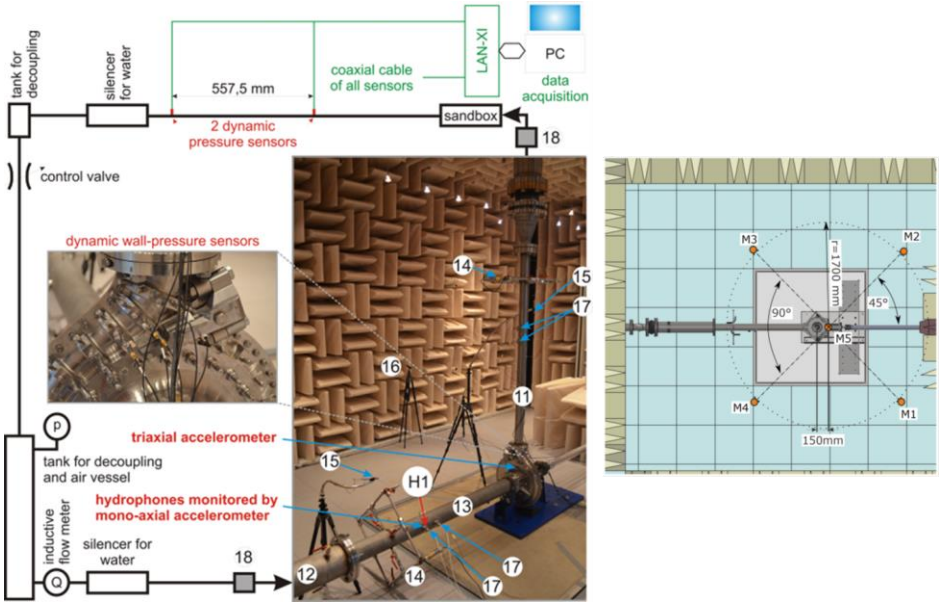

Fig.1 left: Integration of the pump into the semi anechoic chamber (Witte et al. 2016)
right: Hydrophone adapter and integration in the suction pipe
labels: M1-M5 microphones; 11 discharge pipe; 12 flow straightener; 13 suction pipe; 14 ring line for static pressure measurements; 15 microphone; 16 optical speed sensor; 17 dynamic pressure sensors or hydrophones (H1)

The experimental setup used in this study has been presented in Witte et al. (2016) and Bleeck et al. (2016); see Fig.1. The features of the used single stage radial pump and geometrical main parameters of the rotor can be extracted from Fig.2. The complete setup was installed in a semi anechoic chamber to fulfill the special needs of acoustic measurements. The drive of the pump was inside of the chamber as well but was mechanical decoupled and encapsulated by an acoustic insulation. Measurements of the background noise of the pump drive were just little above noise floor of the used microphones of around 16dB(A). Thus, a noteworthy influence on the results of the noise emission measurements from the pump itself can be ruled out. The pump can be equipped with dynamic pressure sensors to measure wall pressure fluctuations in the volute and the rear side chambers. In total 94 measurement positions are available. The measurement uncertainty of the used dynamic pressure sensor is around than 1% which has been tested by a factory calibration. The inner surface of the volute which has a complex 3D curvature was flattened respectively planed by milling in the vicinity of the mounting holes for the pressure sensors. This ensures that the head of the sensor element and the volute surface are perfectly aligned in a plane. Artificial disturbances in the flow field introduced by the sensor head can be ruled out. These slight geometrical modifications of the volute surface were considered in the CFD model as well. The emission of hydroacoustic noise into the connected pipe system can be measured at various positions with dynamic pressure sensors or with hydrophones. The emission of airborne noise was measured on 5 positions around the pump inside the anechoic chamber. The microphones were therefore placed on the virtual surface of a semi sphere with a radius of 1700 mm. Tri-axial acceleration sensors were used for the experimental modal analysis as well as for the determination of the ODS during operations. The accelerations of the pump housing were measured at more than 300 different locations to determine the ODS. The accelerations sensors were mounted using magnetic pads which ensure a proper phase and amplitude lock between sensor and pump housing up to 1500 Hz. Furthermore, all sensors elements underwent an amplitude calibration at 250 Hz leading up to a 3% measurement uncertainty. The acquisition was done synchronously for all measurement quantities with a sampling frequency of 65 kHz with Brüel & Kjaer's LAN-XI system. The post processing of the measurement data was done consistently with in-house software tools except for the modal analysis.

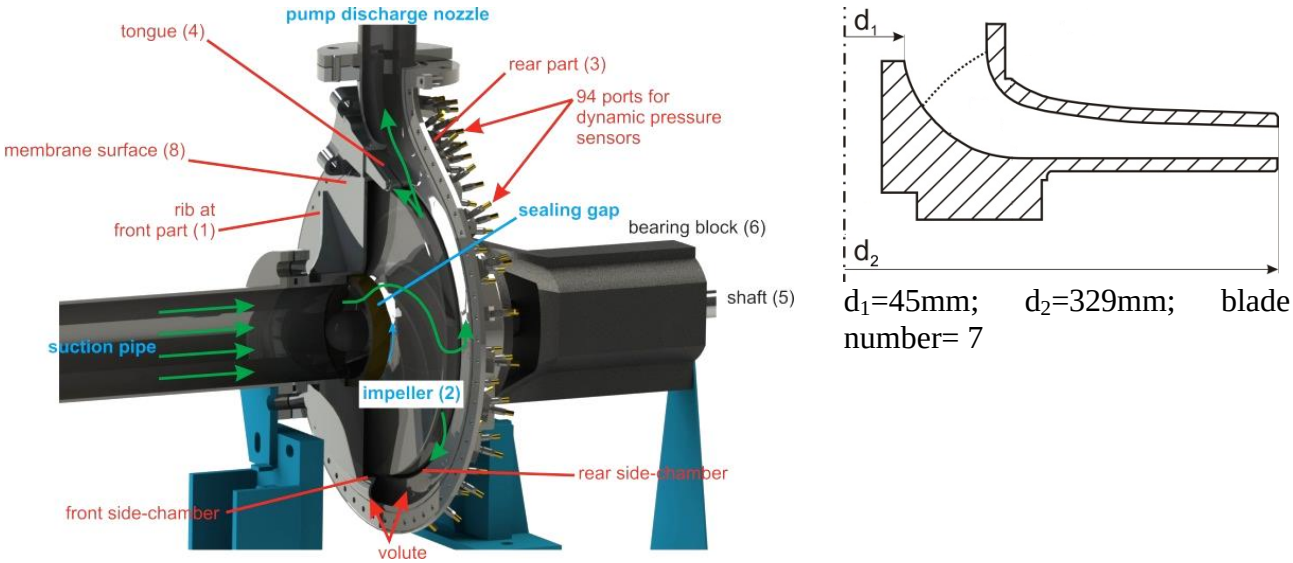

d_1=45mm; d_2=329mm; blade number= 7

Fig.2 left: Geometrical main parameters of the pump
right: Main rotor parameters

SETUP FOR CFD ANALYSIS

The computational model used for this study contains all hydraulic components of the radial pump, namely suction and discharge pipelines, rotor, casing (volute), side chambers, and the sealing gap.

Parts of the simulated turbomachine are displayed in Fig.3. It was assured that the structured hexahedral mesh fulfills all critical mesh parameters (orthogonal angle, aspect ratio, mesh expansion factor); see Tab.2. Stationary and rotating mesh parts were coupled by General Grid Interfaces (GGI). The commercial code ANSYS CFX was used for this study to solve the incompressible three dimensional unsteady Reynolds-Averaged-Navier-Stokes equations. A bounded central differencing scheme (BCDS) was used to discretize advection and diffusive fluxes which is second order. An implicit second order scheme was used for the time integration of the governing equations. The solution of the equation system was done in an agglomeration based multigrid framework simultaneously for all quantities.

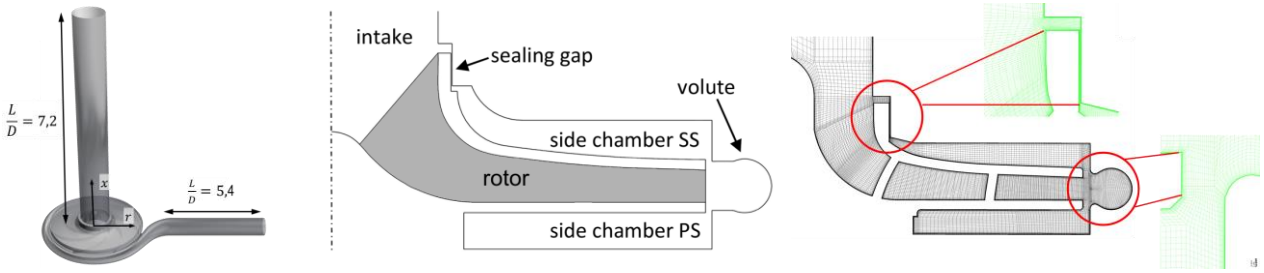

Fig.3 left and middle: basic parts of the CFD model; right: meridional cut of the structured hexahedral mesh

The k-ω-SST-SAS turbulence model was applied for closure of the unknown turbulent Reynolds stress tensor. In general, the SAS is an extension of Menter's original k-ω-SST model wherein an additional source term is added to the transport equation of the specific dissipation rate ω pushing this model to be less dissipative and thus resolving more turbulent motion patterns; see (Menter, F. R. and Egorov, Y. (2010), ANSYS Inc. (2013)). Effects by strong streamline curvature were accounted for with a correction scheme according to Smirnov and Menter (2014). Furthermore, at this state of the investigations the chosen turbulence model seems to be a good compromise between scale resolving capabilities and numerical effort. More advanced Detached Eddy Simulations (DES-SBES) are currently in progress but will be not discussed at this point. Generally, the DES operates in the URANS mode within the boundary layer where the pressure gradient vanishes in wall normal direction. The core flow besides the boundary layer is computed in the Large Eddy mode (LES). Pressure fluctuations from resolved unsteady flow structures in the LES region close to the boundary layer will therefore impressing the wall pressure field. This might be an advantage of the DES compared to the more dissipative SAS approach to compute wall pressure fluctuations more precisely which is essential for the prediction of the noise generation and emission.

Tab.2 CFD mesh parameters

mean y^+	0,9
max. mesh expansion factor	33
min. angle [°]	25
mean aspect ratio	< 5 for 88% of all cells; max. value 3652
element number	62 Mio.

The time step was chosen to be $\Delta t = 1.5 \cdot 10^{-5}\ s$, which corresponds to a rotational increment of 0.15° of the rotating mesh part. The chosen time step width ensures that the RMS Courant number computed over the computational domain remains in an acceptable range. The static pressure and Neumann conditions (zero gradients) for turbulence quantities were used as boundary conditions at the domain inlet. The mass flow rate was specified at the domain outlet with Q = 64.5 m^3/h at a rotational speed of n = 1450 min^{-1} which is the best efficiency point. All walls in the computational model were assumed to be hydraulic smooth. The unsteady wall pressure fields were written for

each time steps after monitored integral quantities like head or efficiency as well as pressure and velocity values at certain grid points were converged. In total, 10400 unsteady wall pressure fields were used for the subsequent FEM analysis which corresponds to around 4.3 revolutions of the rotor.

The assumption of an incompressible fluid made for this analysis is valid because within the pump the incompressible pressure fluctuations p^{inc} are much higher than the compressible, hydroacoustic fluctuations p^{ac}. The wall pressure field will be therefore dominated by p^{inc} and will be used for the FEM analysis only. The incompressible fluctuations will be continuously damped out by dissipation processes when the flow enters the pipes of a hydraulic network. Thus the compressible part becomes dominant downstream from the source of the pressure pulsations and has to be considered when the pressure excitation of the hydraulic pipe system should be analyzed. The compressible fluctuations can be computed from incompressible CFD results with the EIF procedure developed by Hardin and Pope (1994) in this case.

SETUP FOR FEM ANALYSIS

The wall pressure fluctuations from the URANS simulation were used as excitation forces for the FEM based ODS as described in the previous section. The FEM model was derived from the CAD geometry of the radial pump. The 94 mounting holes used for the application of the dynamic wall pressure sensors were removed from the CAD to simplify the geometry for the mesh generation to keep the total finite element number in an acceptable range. The influence of the drive shaft was furthermore simplified by the used boundary conditions at point P 5 wherein the degree of freedom in x-direction was blocked. Further simplifications were not applied to the finite element model to ensure a comparability with the experimental setup as close as possible. The setup for the FEM model is shown in Fig.4 (left) and is as close as possible in accordance to the realized experimental setup.

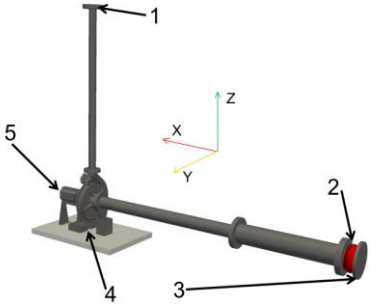

FEM boundary conditions:
P1 P3 and P4: $u_x = 0$; $u_y = 0$; $u_z = 0$
P2: compensator stiffness variable
P5: $u_x = 0$; u_y = free; u_z = free

Fig.4 boundary conditions for FEM model

$$\begin{bmatrix} [M] & [0] \\ [M^{fs}] & [M^{P}] \end{bmatrix} \begin{Bmatrix} \{\ddot{u}\} \\ \{\ddot{p}\} \end{Bmatrix} + \begin{bmatrix} [C] & [0] \\ [0] & [C^{P}] \end{bmatrix} \begin{Bmatrix} \{\dot{u}\} \\ \{\dot{p}\} \end{Bmatrix} + \begin{bmatrix} [K] & [K^{fs}] \\ [0] & [K^{P}] \end{bmatrix} \begin{Bmatrix} \{u\} \\ \{p\} \end{Bmatrix} = \begin{bmatrix} \{F\} \\ \{0\} \end{bmatrix} \quad \text{Eq.1}$$

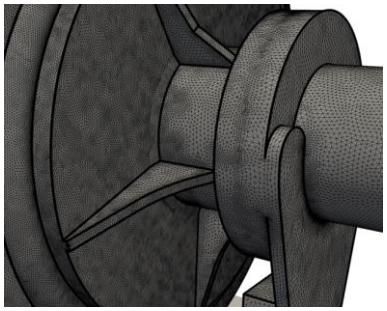
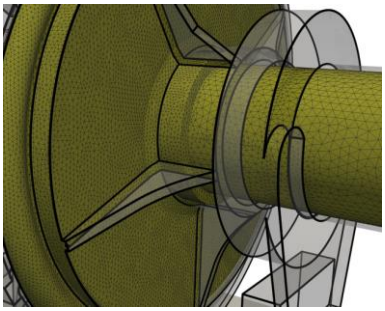

Fig.5 left: structural FEM mesh; right: mesh of the inner fluid cavity

Furthermore, we have to consider that this is an coupled acoustic-structural problem which arises from the fact that the material densities of steel ($\rho_{Steel} \approx 7.8$ g/cm^3) and water ($\rho_{Water} \approx 1$ g/cm^3) are close. In this case, the coupled FEM equations (Eq.1) are not symetrical and dense. In addition to the well known structural matrices M (mass), damping (C) and stiffness (K) we have to consider the fluid counterpart M^P, C^P and K^P as well as the coupling matrices M^{fs} and K^{fs}. The wall pressure distribution from the k-ω-SST SAS is included in the nodal force vector F. Consequently, the structural part of the pump and the inner fluid cavity have to be discretized by FE-elements (Fig.5).
An semi automatic tetrahedral meshing technique was applied for mesh generation to ensure that a proper finite element mesh was generated. Furthermore, it is important that finite elements with quadratic shape functions (Tetra10) are used only to avoid numerical induced stiffness problems. The displacement boundary conditions and the stiffness of the rubber compensator in the finite element model were determined in a iterative fashion so that the natural frequencies and mode shapes from the experimental modal analysis were in accordance with the numerical results. A manipulation of the mass or stiffness matrices finite element model has not been done. This manual model update was done by neglecting the influence of the fluid filling which has reduced the computational effort tremendously. Of course, the experimental modal analysis which provided the validation data was also done without the fluid filling of the pump for this case. The fluid elements in the finite element model have been activated later after the initial modal updating was done. The comparision of the experimental and numerical determined natural frequencies revealed that the deviation is in the range between 1 % – 6 %, see Tab.3. The accordance of the mode shapes were checked visualy. Additional tests were done for the pump casing only to determine the model sensitivity regarding the influence of the fluid filled pump cavity with respect to the natural frequencies; see Fig.6. The analysis showed that the natural frequencies are generally lower when the fluid domain is active in the finite element model which is expectable. Nevertheless, the differences are low and the mode shapes are quite equal at least in the frequency range up to 500 Hz. The influence of the fluid filling is getting more obvious for higher frequencies thus the deviation of the mode shapes and the natural frequencies increases.

Tab.3 Comparison natural frequencies from experiment and finite element analysis

experiment [Hz]	234	247	333	432	469	509	592	905	988	1132	1267
FE analysis [Hz]	243	255	353	438	472	518	584	928	999	1139	1283
deviation [%]	3.7	3.1	5.7	1.4	0.6	1.7	-1.4	2.5	1.1	0.6	1.2

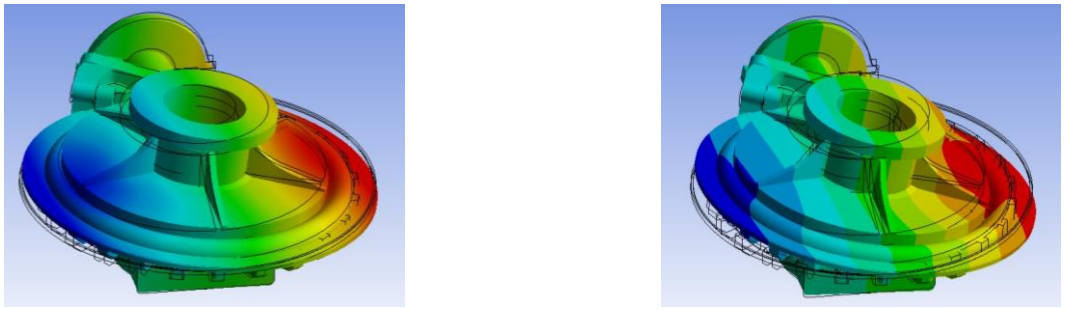

Fig.6 left: mode shape at 245Hz with active FE fluid domain
right: mode shape at 256Hz with deactivated FE fluid domain

The set of equations (Eq.1) were solved in the frequency domain for pressure excitations at specific orders of the BPF to obtain the operational deflection shapes which reduces the computational effort compared to a solution in the time domain. The applied procedure for one way coupling of the fluid dynamic and structural simulation is valid as long as the structural deflections do not affect the flow field or the wall pressure distribution. The applied procedure for one way coupling of the fluid dynamic and structural simulation is valid as long as the deflections of the pump housing do not affect the flow field or the wall pressure distribution. The transformation of the wall pressure field

into the frequency domain requires an stationary process but enables the selective inspection of the ODS for different frequencies thus the finite element analysis has not to be done for all time steps of the CFD simulation.

RESULTS

The results of the CFD and FEM simulations as well as the experimental results will be discussed in this section. The comparison of the pump head H in Tab.4 reveals that the k-ω-SST SAS underpredict the flow losses in the pump slightly by 3.3 %. The pressure head was measured according to DIN EN ISO 9906:2012 class 1 with a uncertainty of 1.5 %. The time history of the pump head and the amplitude spectrum are shown in Fig.7. According to the highly unsteady nature of the turbulent flow field pronounced fluctuations in the head can be inspected. The transformation into the frequency domain indicates that most of the fluctuations in the pump head signal are related to the different orders of the BPF; see Fig.7. The highest fluctuations are observable at the 1th BPF order (f/n = 7) and getting successively smaller for the following ones. Fluctuations in the pressure field which can be observed at every point in the flow field with a similar spectrum as shown in Fig.7 will therefore affect the spectrum of the pressure head as well.

Tab.4 Comparison of the pump head H between the experiment and the numerical solution

	H [m]	RMS [m]
experiment	37,7	0,2
CFD	39,0	0,7

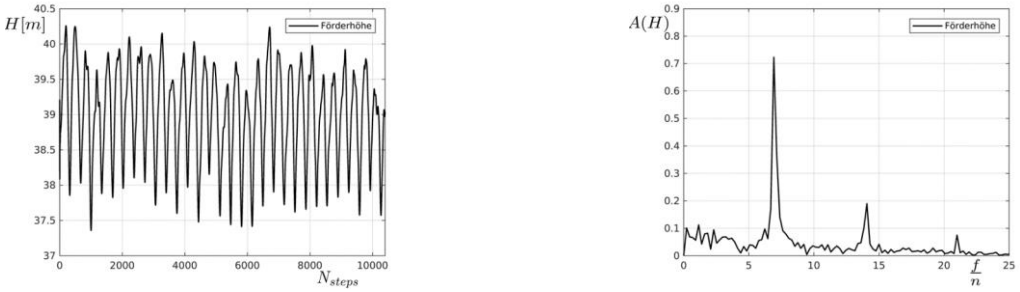

Fig.7 left: time history of pump head; right: frequency spectrum of the head

Frequency analysis of the measured pressure head have not been done because the used ring line and the very small surface drill holes for the static pressure measurements would tamper the fluctuations or even damped them completely out.

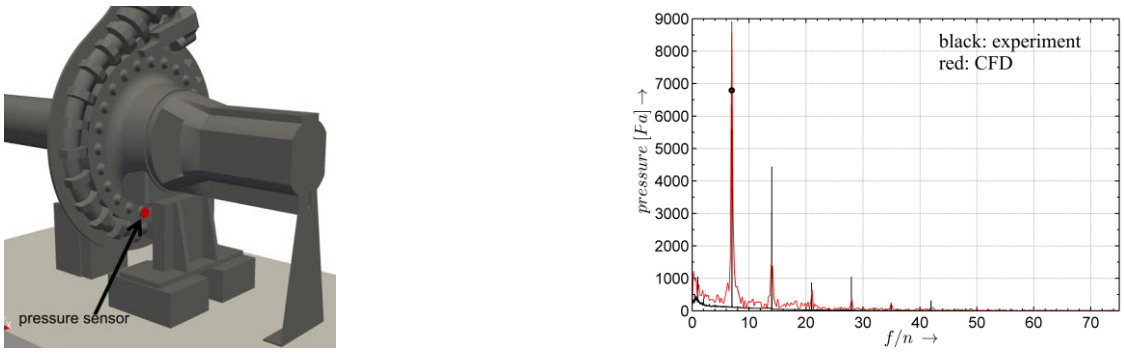

Fig.8 left: position wall pressure sensor; right: comparison between experiment and CFD

The results from the pointwise measurements of the wall pressure fluctuation (Fig.8 left) show that the CFD simulation over estimates the fluctuation level at the 1th BPF order by 23 % though the

fluctuation amplitudes are underestimated for successively higher BPF orders (Fig.8 right). Despite the fact that the used turbulence model is designed with scale resolving capabilities the core of this method relies still on the conventional URANS k-ω-SST model which might be one reason for the underestimation of the wall pressure fluctuation. The turbulent vortex structures which are inherently connected with the pressure pulsation in the flow field are shown as iso-surfaces of Hunt's Q criterion in Fig.9 (left) in the volute casing. The value of Q was normalized by the rotor diameter d_2 and the circumferential velocity u_2 and was chosen as high as possible in order to visualize selectively the very dominant flow structures in the field. A pronounced pattern in the computed Q field can be seen behind the trailing edge of the blades especially in the second half of the volute measured counter clockwise from the tongue position. A detailed view of the trailing edge wake flow structures is given in Fig.9 (right). The development of the vortex structures is initiated right behind the trailing edge and is the result of the complex interaction by both free shear layers which develop from the boundary layer on the blade suction and pressure side; see Fig.9 (right). Especially in the vicinity of the tongue a strong amplification in the wall pressure fluctuations by the different superimposed and tightened flow structures can be observed; see Fig.10.

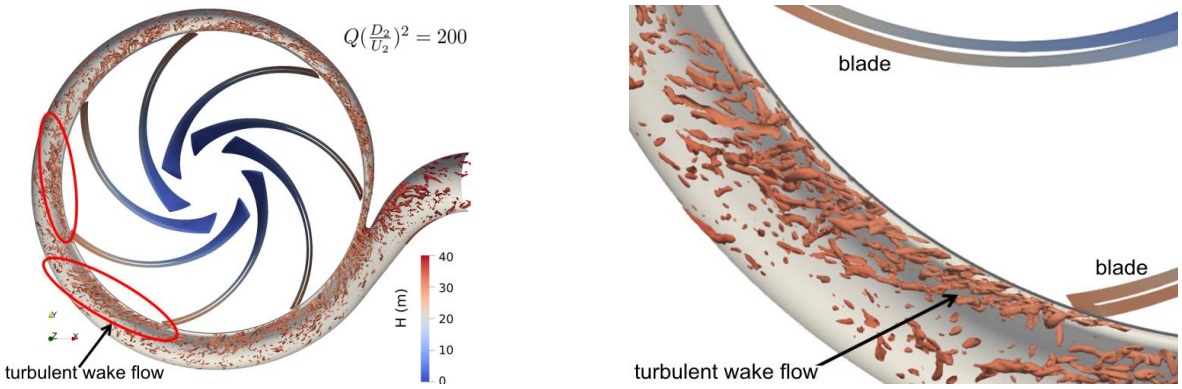

Fig.9 left: vortex structures in the volute; right: wake flow behind blade trailing edge

The real part of the Fourier transformed wall pressure field from the CFD simulation is shown for different normalized frequencies respectively BPF orders in both figures. The spatial wavelength of the periodic pressure pattern in the Fig.10 (left) is in accordance with the 1th order of the BPF thus 7 changes in the sign of the pressure pattern are present. A close inspection reveals that the highest amplitudes are in affect at the tongue position. Furthermore, the periodic pressure pattern propagates with slow decreasing amplitudes into the discharge pipe. The rear and front part of the side chambers are affected by the fluctuations of the wall pressure field as well.

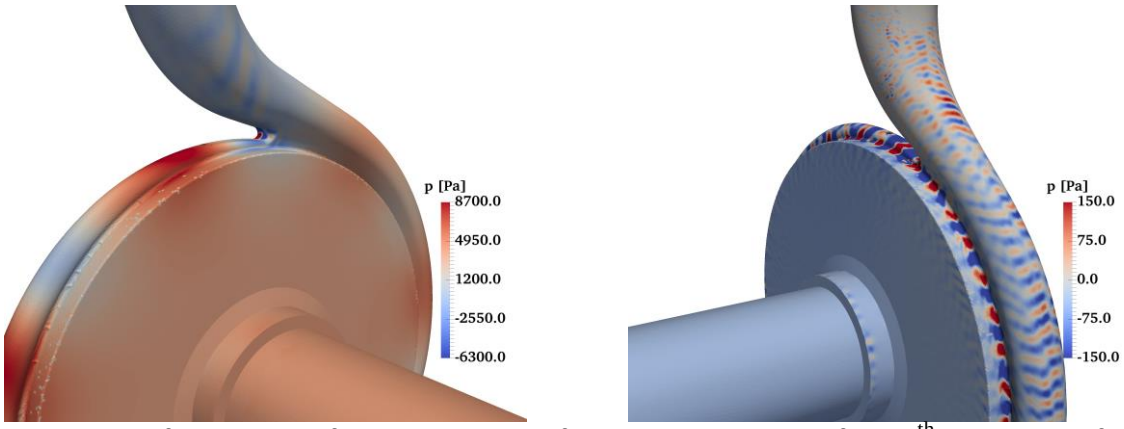

Fig.10 left: real part of the Fourier transformed wall pressure field 1th BPF order (f/n = 7)
right: real part of the Fourier transformed wall pressure field 6th BPF order (f/n = 42)

The spatial wavelength of the pressure pattern and the amplitude are continuously reduced for higher BPF orders; see Fig.10 (right). Even when the amplitudes are quite low pulsations of the wall pressure field can be identified in the inlet region and all over the side chamber area. So far we can constitute that especially the tongue, respectively the close-up region around the tongue, is characterized by the highest amplitudes of the wall pressure field, for which reason the highest structural excitation forces can be expected in that region as well. The structural stiffness of the casing region around the tongue is therefore an important factor for its contribution to the airborne noise emission. Even if the direct contribution to the airborne noise is low the tongue as a strong acoustic dipole is at least relevant for the radiation of hydro acoustic noise into the connected hydraulic system. Although the pressure pulsations are significantly reduced at the volute wall, this region, together with the side chambers, seems to be more important for the airborne noise emission of the pump, because the structural stiffness of this casing part is normally not as high as for the tongue region.

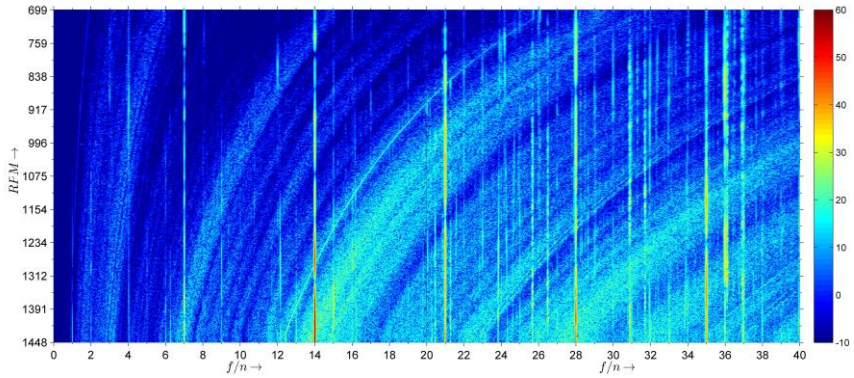

Fig.11 Campbell chart for microphone M3 (position see Fig.1) from experiment
Q_{Max} = 64.5 m^3/h at speed n = 1450min^{-1}
color coding top row: sound pressure level L_P A-weighted

In accordance to the computed and measured wall pressure pulsations the highest share in the airborne noise emission is also situated along the different orders of the BPF; see Fig.11. The curved bands with slightly increased sound pressure levels in the Campbell order chart reflecting the excited natural frequencies of the pump. Once the BPF matches a natural frequency respectively is crossing one of those bands respectively the sound pressure level will raise.
Once the wall pressure fields were transformed in the frequency domain they were fed into the finite element model of the pump as nodal excitation forces to compute the corresponding ODS. This has been done without an active fluid domain in the FEM model so far. Despite of that, the operational deflection shapes will be discussed and compared with the experimental results obtained for the 1^{th} and 2^{th} order of the BPF. The operational shapes for an excitation frequency at the 1^{th} BPF order (f/n = 4) are shown in Fig.12 (top row).
The deflection in Z direction is color-coded and the deformation of the pump geometry has been scaled individually for the experimental and FEM results to allow a reasonable visualization of the operational shapes. The main vibration behavior of the pump at this frequency is mostly equal between the FEM solution and the experimental result. The suction pipe bends mostly in Y direction which is superimposed by a deflection with low amplitude in X direction. The superposition led to a revolving motion of the suction pipe around the pipe axis. The main bending direction of the discharge pipe is the Y direction as well superimposed by a deflection component in Z direction thus the revolving motion pattern along the X axis can be identified. The deflection patterns of suction and discharge pipe are in phase. The deflection of the front part of the pump casing is dominated by a deflection component in Z direction. It can be seen in Fig.12 that the FEM solution predicts a mostly homogenous deflection in Z direction over the entire front casing part. The measurement reveals a slightly other behavior wherein the upper and lower part of the front casing

show a phase shift of 180°. Thus the upper part moves backwards in Z direction (blue color) and the lower part moves forward (red color). The ODS for the 2th BPF order differs significantly from the 1th BPF order.

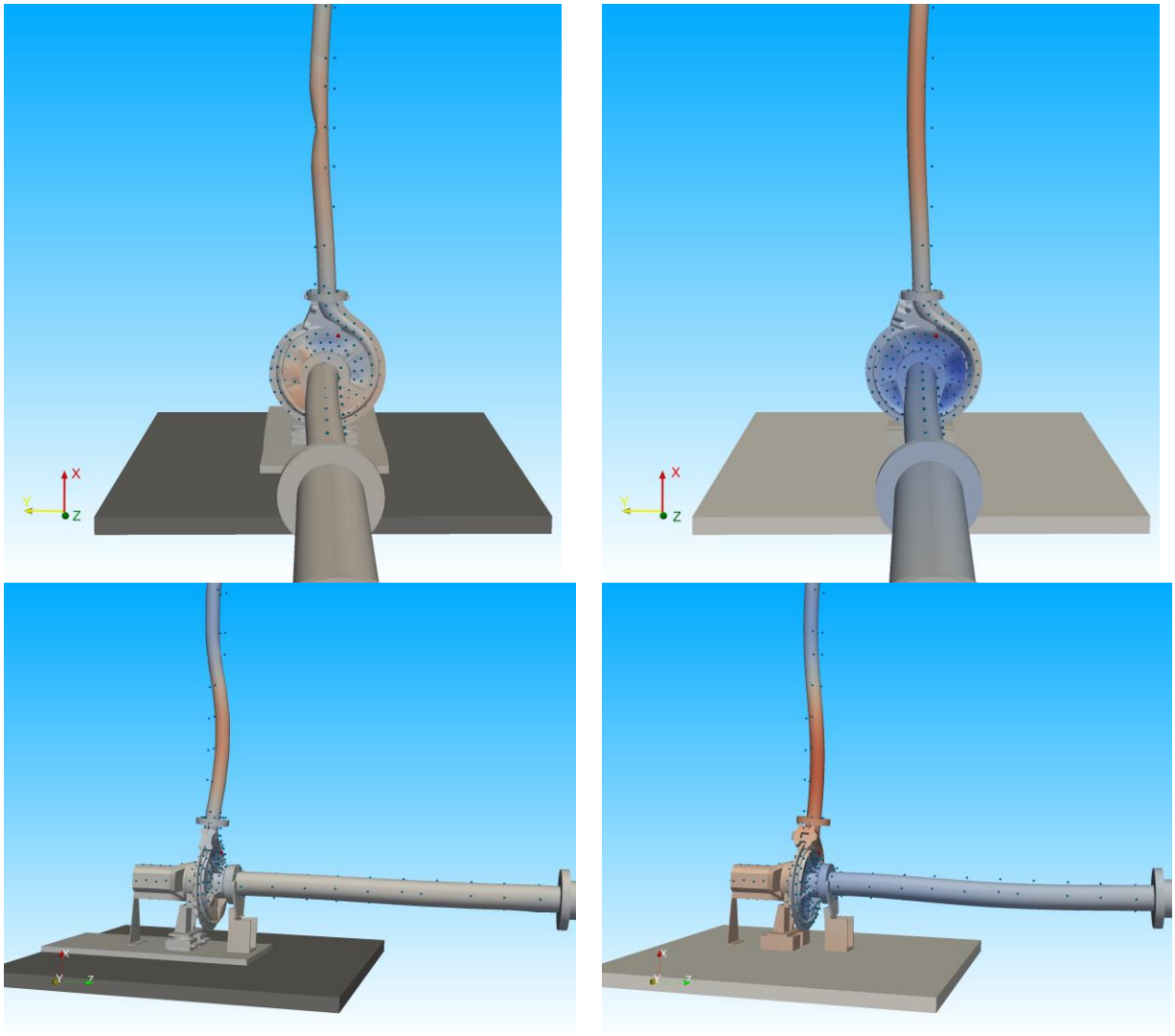

Fig.12 Operational Deflections Shapes
top row: experiment left – FEM right; frequency: 1th BPF order (f/n = 7)
bottom row: experiment left – FEM right; frequency: 2th BPF order (f/n = 14)
blue point = locations of the acceleration sensor in the experiment;
color: deflection in z direction

The deflection pattern is not superimposed by a motion component perpendicular to the X-Z plane for the FEM result in contrast to the first case thus no revolving motion of the pipes around their axis can be inspected. This is also the case for the suction pipe in the experiment but not for the discharge pipe where at least a small perpendicular deflection component can be observed which results in a small orbiting motion around the pipe axis. Additionally, it can be seen that the bending pattern of the discharge pipe is characterized by a node in the middle of the pipe caused by the higher excitation frequency in this case. The strong bending of the pipe causes strong deformations in the pressure flange region of the pump as well. The bending behavior of the casing front part is dominated by a uniform deflection component in Z direction. Once again, a phase shift is recognizable in the experiment between upper and lower part which will be investigated in the next measurement campaign in depth. The deformation for the rear part of the pump casing is negligible for excitations at the 1th and 2th BPF order because the structural stiffness of this pump part is very

high. Nevertheless, despite the good accordance of the ODS shapes the deformation amplitudes are slightly over estimated by the FEM model because up to this point the influence of the fluid has not been taken into account. This will be done in future to obtain the correct sound pressure amplitude from a BEM airborne noise simulation.

CONCLUSIONS

The present study investigated different aspect which causes the emission of hydro acoustic and airborne noise of a single stage radial pump. A comprehensive experimental setup within a semi anechoic chamber was introduced installed capable to measure all important physical quantities in the noise generation and emission process. The experimental investigations of the wall pressure fluctuations, the operational deflection shapes and the airborne noise emission of the pump were flanked by CFD and FEM analysis. A scale resolving CFD method (k-ω-SST SAS) was utilized to compute the unsteady pressure and velocity fields inside the pump. The comparison of the wall pressure fluctuations from the CFD analysis with experimental results revealed that the SAS is capable to simulate the unsteady wall pressure fields with distinctive fluctuation components at the different orders of the BPF. A detailed comparison of the amplitudes at the BPF orders showed that the SAS underestimates these fluctuations in most of the cases except for the 1^{th} BPF order. The analysis of the unsteady velocity fields in the volute of the pump showed that especially in the wake flow of the rotor blades pronounced vortex structures are present. In the vicinity of the tongue these structures are responsible for the development of very high pressure fluctuation at the BPF orders which was observed from the Fourier transformed wall pressure fields. Therefore, the tongue region is one of the primary acoustic dipole sources for the hydro noise emission into the connected hydraulic system of the pump. However, the volute casing and the side chambers are surely the most prone regions for structural vibrations and airborne noise emission because the structural stiffness is reduced compared to the tongue region. The wall pressure fluctuations have been used to compute the ODS using a finite element model of the pump. The natural frequencies and mode shapes of the FEM model were updated to the experimental results by adjusting the FEM boundary conditions. The deviation of the natural frequencies between the experiment and the FEM solution was in the range of 1% – 6% depending on the mode shape. The computed ODS at the 1^{th} and 2^{th} BPF order were in accordance with the experimental results except the deformation amplitudes. Generally, the deformation amplitudes were slightly over estimated by the FEM model when the fluid part in the model was not activated. The fluid part in the FEM simulation will be considered in future investigations in conjunction with further adjustments of the FEM model, additional experimental investigations and the switch to a detached eddy simulation setup for the flow field analysis. The BEM simulation of the airborne noise and the simulation of the hydro acoustic noise using the EIF approach will be further steps in the upcoming investigations.

ACKNOWLEDGEMENTS

The authors are grateful for the funding of the project by the “VDMA FV Pumpen und Systeme” and want to thank the members of the committee for the constructive discussions.

REFERENCES

ANSYS INC., (2013) *CFX-Solver Theory Guide (Release 15.0)*, Chap. 2.7.

Berten, S., Farhat, M., Avellan, F. und Dupont P., (2007). *Rotor-Stator Interaction Induced Pressure Fluctuations: CFD and Hydroacoustic Simulations in the Stationary Components of a Multistage Centrifugal Pump*. AIAA. 1994. Proceedings of FEDSM2007

Darvish, M., Frank, S. und Paschereit, C. O., (2015) *Numerical and Experimental Study on the Tonal Noise Generation of a Radial Fan*. Journal of Turbomachinery, 137

Dong, R., Chu, S. und Katz, J., (1997) *Effect of modification to tongue and impeller geometry on unsteady flow, pressure fluctuations, and noise in a centrifugal pump*. Journal of Turbomachinery, 119

Hardin, J. C. and Pope, D. S. (1994) *An Acoustic/Viscous Splitting Technique for Computational Aeroacoustics.* Theoretical Computational Fluid Dynamics, Vol. 6, No. 5-6, pp. 323-340.

Jackson, E. D., (1966) *Study of Pump Discharge Pressure Oscillations.* Final Report, Rocketdyne Inc.

Langthjem, M. A. und Olhoff, N., (2004) *A numerical study of flow-induced noise in a two-dimensional centrifugal pump. Part I. Hydrodynamics*. Journal of Fluids and Structures, 19

Langthjem, M. A. und Olhoff, N., (2004) *A numerical study of flow-induced noise in a two-dimensional centrifugal pump. Part II. Hydroacoustics*. Journal of Fluids and Structures, 19

Menter, F. R.; Egorov, Y. (2010): *Scale-Adaptive Simulation Method for Unsteady Flow Predictions. Part 1: Theory and Model Description.* Flow Turbulence and Combustion 85(1), pp.113-138, DOI: 10.1007/s10494-010-9264-5.

Menter, F. R.; Egorov, Y. (2010): *Scale-Adaptive Simulation Method for Unsteady Flow Predictions. Part 2: Application to Aerodynamic Flows.* Flow Turbulence and Combustion 85(1), pp.139-165, DOI: 10.1007/s10494-010-9265-4.

Smirnov, P. E.; Menter, F. R. (2009): *Sensitization of the SST Turbulence Model to Rotation and Curvature by Applying the Spalart-Shur Correction Term*. Journal of Turbomachinery 131(4), DOI: 10.1115/1.3070573.

Strub, R. A., (1964) *Pressure Fluctuations and Fatigue Stresses in Storage Pumps and Pump-Turbines.* ASME. Journal of Engineering for Power, pp. 191-194

Witte, M., Benz, C., Bleeck, S., Wurm, F.-H., (2016) *Principal experimental study of the acoustic behavior of pumps*. Proceedings of the INTER-NOISE 2016 - 45th International Congress and Exposition on Noise Control Engineering: Towards a Quieter Future, pp. 7666-7674.

Bleeck, S.; Benz, C.; Witte, M.; Wurm F.-H., (2016) *Design of an experimental setup to investigate noise generation and radiation of pump systems*. 3rd International Rotating Equipment Conference, Düsseldorf

Witte M, Torner B, Wurm F., (2018) *Analysis of Unsteady Flow Structures in a Radial Turbomachine by Using Proper Orthogonal Decomposition*. ASME. Turbo Expo: Power for Land, Sea, and Air, Volume 2A: Turbomachinery ():V02AT45A023. doi:10.1115/GT2018-76596

Zhu, T., Lallier-Daniels, D., Sanjose, M., Moreau, S. und Carolus, T. H., (2016) *Rotating Coherent Flow Structures as a Source for Narrowband Tip Clearance Noise from Axial Fan*. 22nd AIAA/CEAS Aeroacoustics Conference, Lyon, France